Vortex Breakdown in a Closed Cylinder with Rotating Bottom Disk

Kamal Poddar[1], Navneet Kumar[1], Deepakkumar M Sharma[2]*

[1]Indian Institute of Technology Kanpur, Dept. Aerospace Engineering, Kanpur, India

[2] TSI Instruments India Private Limited, Bangalore, India

*deepak.sharma@tsi.com

Abstract

The swirling flow in a closed cylindrical container with rotating bottom disk was experimentally studied to understand the formation, development, and breakdown vortex bubble. Laser induced Rhodamine dye flow visualization technique and PIV were used to study the vortical flow. The flow behavior has been characterized by aspect ratio ($AR = H/R$) and Reynolds number ($Re = {\Omega R^2}/{\nu}$). Stability limit and condition for appearance of vortex breakdown defined by Vogel (1968) and Escuider (1984) has been confirmed. Control of vortex breakdown using clockwise and counter clockwise rotation of a thin solid central rod ($r/R > 0.1$) near the cylinder axis is also explored.

Nomenclature

AR = Aspect Ratio
VB = Vortex Breakdown
Ω = Angular Velocity in rad/sec
R = Inner Radius of Cylinder
H = Height of Cylinder
ν = Kinematic Viscosity of glycerine/water mixture
r = Radius of thin solid cylinder
Re = Reynolds Number
Φ = Diameter

1 Introduction

The swirling flow generated in a closed cylindrical container by rotating bottom disk, under certain conditions, leads to the formation of one or more recirculation bubbles, centered on cylinder axis. This flow has been characterized by the aspect ratio (${H}/{R}$) and Reynolds number (${\Omega R^2}/{\nu}$). The rotating disk draws in fluid axially and drives it away in an outward spiral in a closed container. This fluid swirls along the cylindrical wall, spirals in across the stationary top disk and then again turns to the axial direction towards the rotating bottom disk. This inward spiral motion results in an initial increment of swirl velocity and concentrated vortex is created due to the conservation of angular momentum. The vortex breakdown mechanism and its control has been studied in confined flow due to several advantages. For example this has well defined boundary conditions, well defined control parameters, and absence of ambient disturbances.

Escuider (1984) revealed a variety of vortex breakdown patterns and their dependence on the disk Reynolds number and aspect ratio of the closed cylindrical container. Vogel (1968), Leibovich (1978) and

few other researchers have modified this base flow in different ways to explore the vortex breakdown mechanism. Spohn (1993) and Brons et al. (2004) have studied a flow driven by rotating bottom disk, with the top surface being free. Experimental and numerical studies have also been carried out with independent rotation of both top and bottom disk. Mullin et al. (2000) used conical central body which was stationary or rotating together with the bottom disk. Husain et al. (2003) studied a new means of vortex breakdown control by using co and counter rotation of a thin solid central rod near the cylinder axis.

The objective of the present work is to study the formation, development, and breakdown of vortex bubbles and the effect of Reynolds number and aspect ratio on the vortex bubble dynamics.

2 Experimental Setup

A borosilicate glass cylinder of inner diameter 140 mm is placed in a rectangular box made of glass. A disk of diameter 139 mm is attached to the shaft drive at the bottom of the cylindrical container. Aspect ratio of cylinder is adjusted by changing the height of the top stationary disk as shown in figure 1. Bottom disk is rotated with a servo DC motor (model-T730-012EL0) which is attached to MID-7654/7652 4/2

Figure 1: Experimental Setup

axis servo motor drive. The motor drive is adjustable in steps of 1 rpm to a maximum of 1600 rpm. The motor rpm is controlled through LabVIEW software. The motor shaft is passed through a mechanical seal to prevent leakage. Instead of pure glycerine, glycerine/water (80/20 by volume) mixture is used to get the reasonable value of kinematic viscosity and rpm.

Temperature of the working fluid is measured with the laser gun thermometer before and after each set of experiment. The working fluid has ν between 63 centistokes to 50 centistokes for the temperature range in between 23°C - 26°C (± 0.5°C). Viscosity of such a mixture is strongly temperature dependent (5-7% change per °C) therefore gap between the rectangular box and cylindrical container is filled with water to ensure stable operating conditions. Small quantity of Rhodamine B dye dissolved in same glycerine/water mixture was injected through a hypodermic syringe into the container through a 1mm dia. hole at the center of the stationary top disk. Flow was illuminated using a 5W continuous green laser (about 1mm thick sheet and wavelength of 501-600 nm) in a diametral plane between the container end walls. NIKON DSLR810 camera (60 frame/second) with Milvus 2/100M lens is used for capturing images and videos.

3 PIV Measurements

In the present study, the velocity field of vortex breakdown bubble and its surrounding area are measured using PIV system. The tracer particle used in this study are glass sphere, without coating, particles with a nominal dia. of 10 μm and specific weight of 0.22 g/cm^3. The particles are illuminated by 1 mm thick laser sheet at a wavelength of 532 nm and maximum energy output of 200 mJ/pulse. The sheet forming optics consists of one cylindrical lens of 15 mm. The sheet is aligned to the diametric plane of the cylindrical container. Pairs of images are captured with high resolution 8-bit TSI Powerview plus 8MP CCD camera with maximum resolution of 3320 × 2496 pixel and frame rate of 8.5 fps. The camera is equipped with a 100 mm lens. This setup gave a range of field of view which varied between 2303 × 1607 and 1636 × 2441 for aspect ratio of 1.5 and 3.5 respectively. Special care was taken to align the laser sheet and camera, as any slight misalignment produces a non-negligible bias in the results. The laser and camera are synchronized by eight channel TSI 610036 laser pulse synchronizer. INSIGHT 4G software has been used for acquiring 200 image pairs at 2 Hz. The time between the two laser pulses is optimized for each rotation rate and 4 to 8.5 milliseconds has been used in order to have a particle displacement within the interrogation window. PIVlab software is used for the analysis of acquired pair of images. The final interrogation window size of the PIV analysis is 128 × 64 pixels which is found to give satisfactory results with an overlap of 50 percent between the windows. The total area of the captured image is 560 mm × 421 mm. The adaptive correlation analysis adopts a multi-grid cross-correlation approach as explained in the previous section. Additionally, the window deforming option is invoked during the adaptive correlation analysis. The validation parameters are used to fine-tune the processing and to remove the spurious vectors. The peak validation is done by setting values for the minimum and the maximum peak widths as well as the minimum peak height ratio (between first and second peaks) and thereby imposing stringent conditions on peak identification for the subsequent determination of vectors. In addition to the peak validation, a local neighborhood validation is used, which is capable of making a realistic estimate of spurious vectors based on neighboring vectors. The software then replaces the spurious vectors that deviate from the specified criteria by interpolation of vectors from the neighboring cells.

4 Results and Discussion

Formation and breakdown of single, double and triple vortex breakdown bubbles are described first. For a particular value of aspect ratio, breakdown bubbles are observed only between certain values of Reynolds number. Visualization results suggest that there is a central viscous core which increases in diameter with increasing distance from the rotating bottom disk.

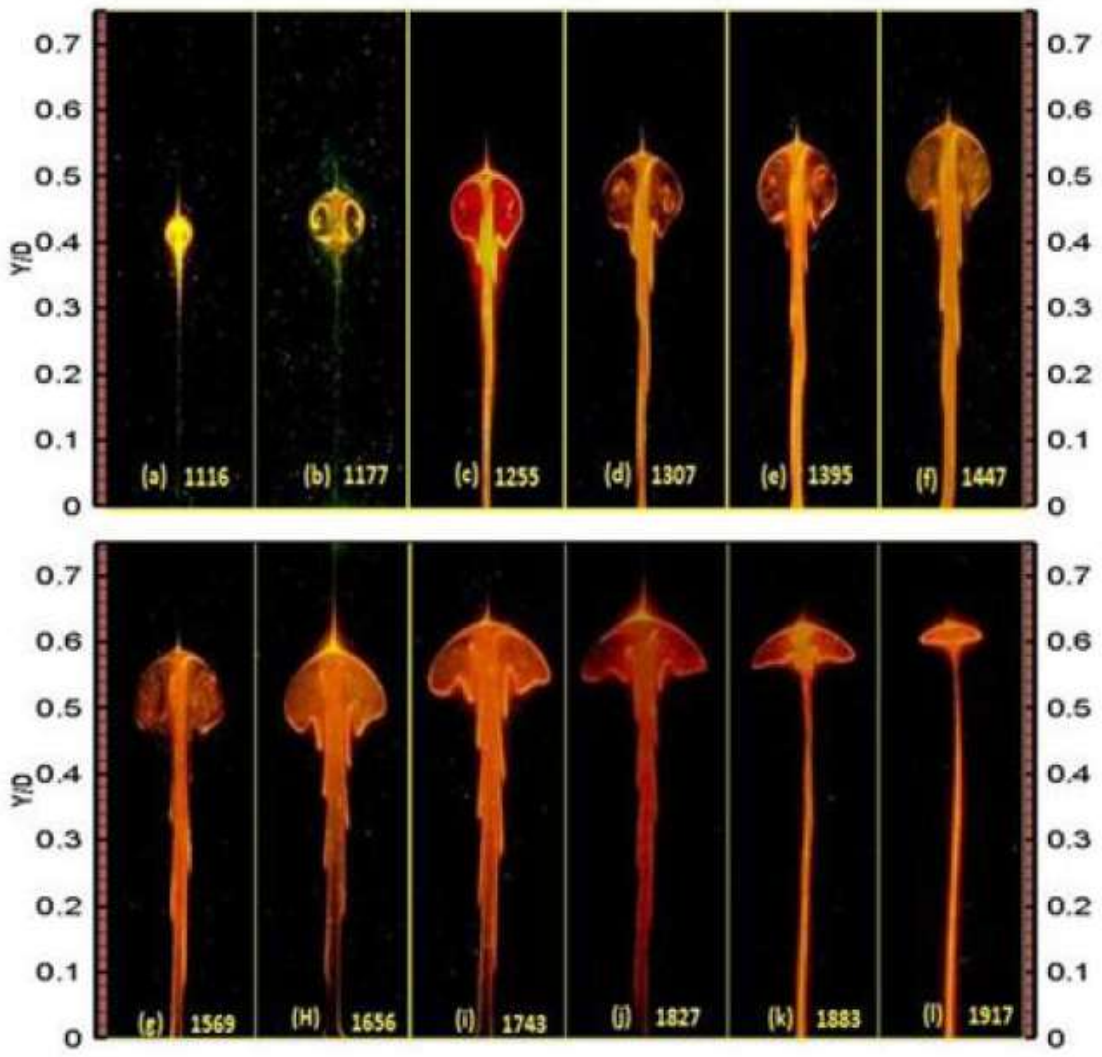

Figure 2: Visualization of vortex breakdown process with increasing *Re* for *AR* = 1.5

In the case of *AR* = 1.5, at low rotation rate (*Re* = 1050) the flow has simple cellular structure. As the rotation rate is increased to *Re* = 1116 (figure 2a), the central filament of dye reveals a short region where the flow comes close to the stagnation. Further increase in rotation rate to *Re* = 1177 (figure 2 (b)) leads to an outer flow which is somewhat different from that of *Re* = 1116. Now there is a well-defined vortex breakdown (a stagnation point upstream of a zone of near stagnant recirculating fluid). A series of twelve photographs of the vortex region are presented in figure 2 to illustrate in more detail the changes which occur with increasing Reynolds number. As the rotation rate is increased vortex breakdown (figure 2 (c-

h)) is more and more radially stretched (size of recirculation zone increases) and moves slightly upward towards the non-rotating disk. When rotational rate Re=1656, size of recirculating zone starts reducing (figure 2 (i-l)) with further increase in rotational rate and when rotational rate reaches *Re* = 2005 then vortex breakdown bubble disappears. For this case of single breakdown, the changes in the size and location of vortex bubble which occurs with increasing Reynolds number are consistent with the results in the published literature.

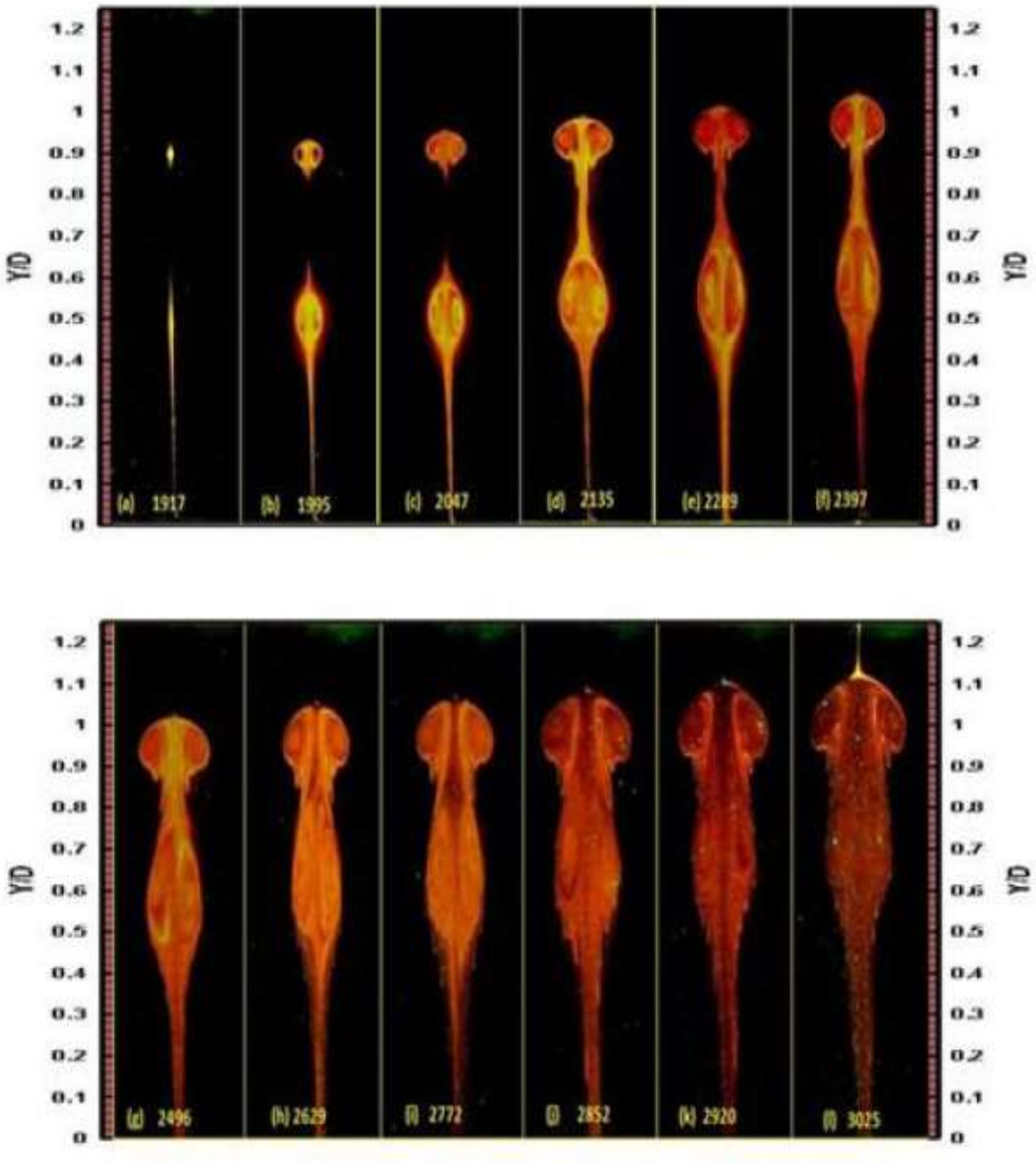

Figure 3: Visualization of vortex breakdown process with increasing *Re* for *AR* = 2.5

For AR = 2.5, stagnation points and recirculation zones are not observed below rotational Re = 1917. Below this rotation rate flow has simple cellular structure similar to the previous case (low Re for AR = 1.5). When rotation rate is increased to Re = 1917 then two upstream and downstream stagnation points appear but recirculation zones are not observed. When rotation rate is further increased to Re = 1995 then there are two well defined vortex breakdown bubbles with distinct recirculation zones (figure 3(b)). Size of recirculation zone i.e. upstream and downstream breakdown bubbles increase with further increase in rotation rate as shown in figure 3(c-l). As Re is increased, downstream breakdown bubble starts oscillating and this oscillation increases with further increase in rotation rate. As the rotation rate is increased, the downstream stagnation point moves towards upstream stagnation point (figure 3 (b-l)) and eventually penetrates the breakdown zone upstream so that at the Re = 2820 there is a single stagnation point with two distinct zones of recirculation.

For double breakdown, it is found that for $AR \leq 2.75$ the upstream breakdown appears first. As the Reynolds number is increased, the downstream stagnation point appears, moves towards and eventually penetrates the breakdown zone upstream so that at the highest Reynolds number there is a single stagnation point with two distinct zones of recirculation. During the experiments it was apparent from the dye movement that the interior of a breakdown bubble represents a zone of very slow recirculation upstream motion at the axis.

PIV technique was employed to the selected rotational rate for each AR. Results at one rotation rate for each AR is discussed in this section. While performing PIV experiments first dye flow visualization image is taken with the help of DSLR camera for the respective rotational rates and then PIV images are captured. This technique is applied so that results of flow visualization and PIV could be compared for the same condition.

For AR = 1.5, first set of images were taken at $\Delta T = 6.5ms$ to capture the global flow and second set of images were taken at $\Delta T = 20ms$ to capture the VB bubble only. Due to large difference in the velocity of VB bubble and global flow, separate set of images were taken to capture the VB bubble only. PIV results i.e. vorticity and velocity field of swirling flow at rotational Re = 1295 are shown in the figure 4. Vorticity contour and velocity vector contour (figure 4(c)) give the location and size of VB bubble and this size and location of VB bubble can be compared with the visualization result (figure 4(a)). Velocity vectors indicate the location of stagnation point. This VB bubble has a pair of vortices and these vortices are counter rotating. Blue color denotes the clockwise rotation whereas red color denotes counter clockwise rotation. At this rotational Re, VB bubble is formed at a distance of 0.4D (60 mm) from the bottom disk (figure 4(c)) and this VB bubble has diameter of 0.2D (28 mm) as shown in figure 4(b). This VB bubble has two counter rotating recirculation zones which are 0.1D (14 mm) in size (figure 4). Stagnation point is located at a distance of 0.5D (70 mm) from the bottom disk as shown in figure 4(b). As the rotation rate is increased size of VB bubble increases and location of stagnation point and VB bubble move towards the non-rotating disk.

There are two more pairs of vortices near the end walls having more axial and radial velocity than VB bubble vortices. Vorticity, axial velocity and radial velocity contours in figure 4 clearly indicate that the swirling flow at this rotation rate is axisymmetric. For higher AR = 2, 2.5 and 3.5 images were taken to

capture the global frame only. Rotational velocity of vortex bubbles are very less as compared to the rotational velocity of the fluid outside the vortex bubbles therefore when ΔT is taken less then flow outside the vortex bubbles are well captured only. Global flow frames give the information about the location and movement of upstream and downstream stagnation points and size of recirculation zones but these frames do not give the information about the flow behavior of interior of vortex breakdown bubbles.

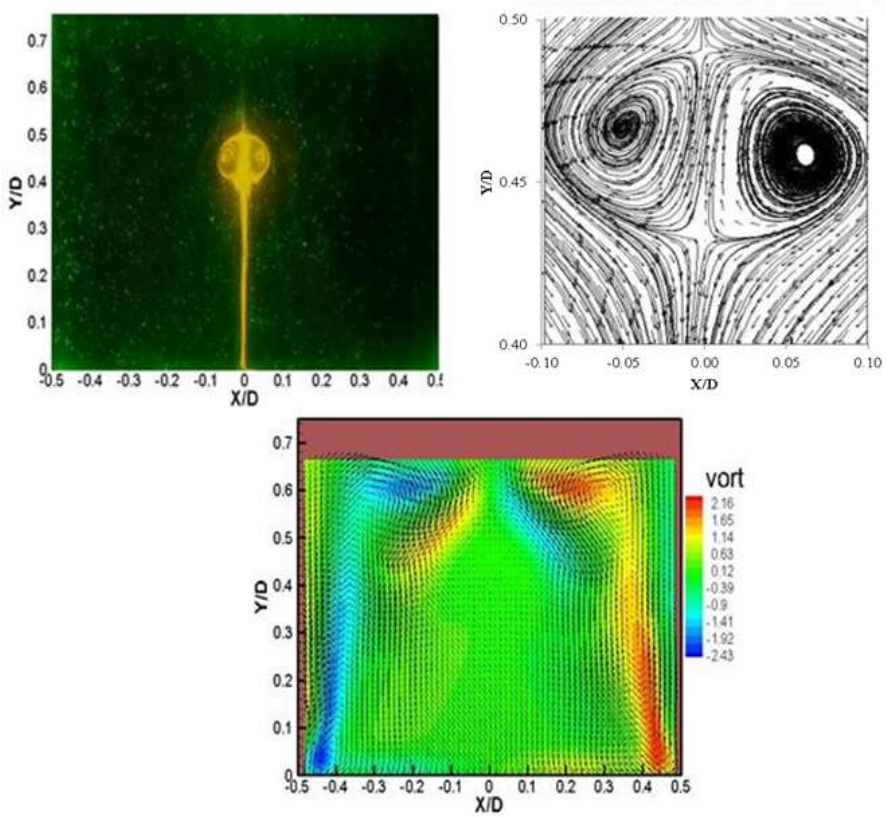

Figure 4: (a) Dye flow visualization (b) Streamline of vortex bubble (c) Vorticity contours along with velocity vector of global flow at *Re* =1295 for *AR* =1.5

For *AR* = 2, velocity vector along with vorticity contours of swirling flow at rotational *Re* = 1787 are shown in the figure 5. Vorticity contour and velocity vector contour (figure 4.8 (b)) give the location and size of *VB* bubble. Velocity vectors at the top in figure 5 (b) indicates the appearance of upstream *VB* bubble and down- stream curved velocity vector denotes the formation of downstream bubble. Upstream *VB* bubble has a pair of vortices (figure 5 (b)) and these vortices are counter rotating while the downstream *VB* bubble has a single vortex. Blue color in all figures denote the clockwise rotation whereas red color denote counter clockwise rotation. At this rotational *Re*, upstream and downstream *VB* bubbles (figure 5 (d)) appear at a distance of 0.6D (90 *mm*) and 0.35D (55 *mm*) respectively from the bottom disk. Upstream and downstream *VB* bubbles are 0.3D (42 *mm*) and 0.1D (14 *mm*) in size respectively (figure 5 (b)). Upstream *VB* bubble has two counter rotating recirculation zones which are 0.15D (21 *mm*) in size. Two stagnation points are located at distances of 0.7D (100 *mm*) and 0.4D (56 *mm*) from the bottom disk as shown in figure 5 (b). As the rotation rate is increased size of *VB* bubble increases, down- stream

stagnation point moves towards the upstream stagnation point and upstream *VB* bubble moves towards the non-rotating disk.

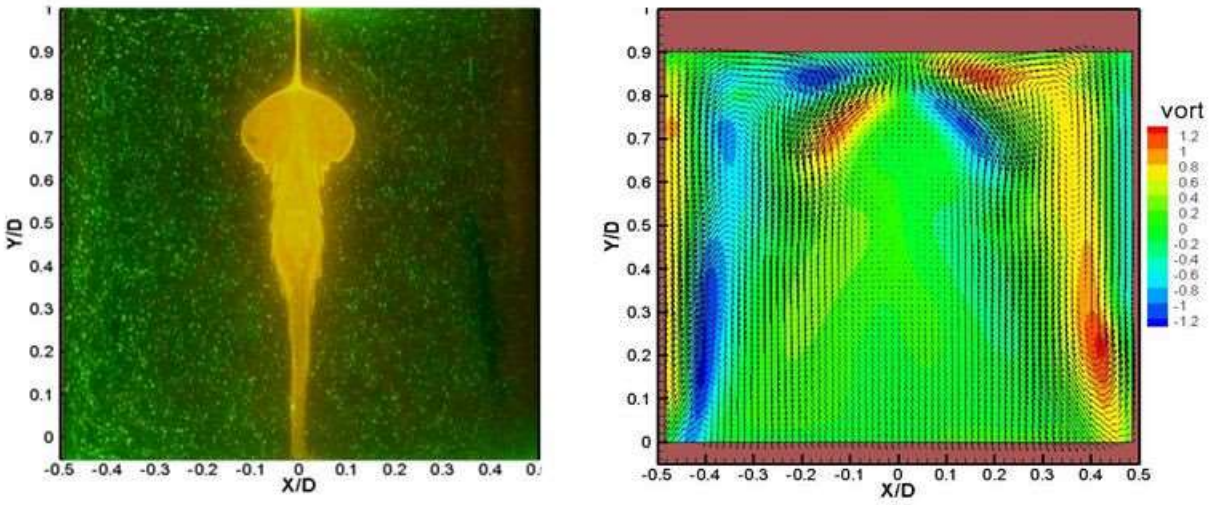

Figure 5: (a) Dye flow visualization (b) Vorticity contours along with velocity vector of global flow at *Re* = 1787 for *AR* = 2.

For *AR* = 2.5, vorticity and velocity contours of swirling flow at rotational *Re* = 2359 are shown in figure 6. Vorticity contour and velocity vector contour (figures 6 (b)) give the location and size of both upstream and downstream *VB* bubbles. Curved velocity vectors at the top in figure 6 (b) denote the recirculation zones of upstream *VB* bubble and downstream curved velocity vector denotes the recirculation zones of downstream bubble. Upstream and downstream *VB* bubbles have a pair of vortices and these vortices are counter rotating.

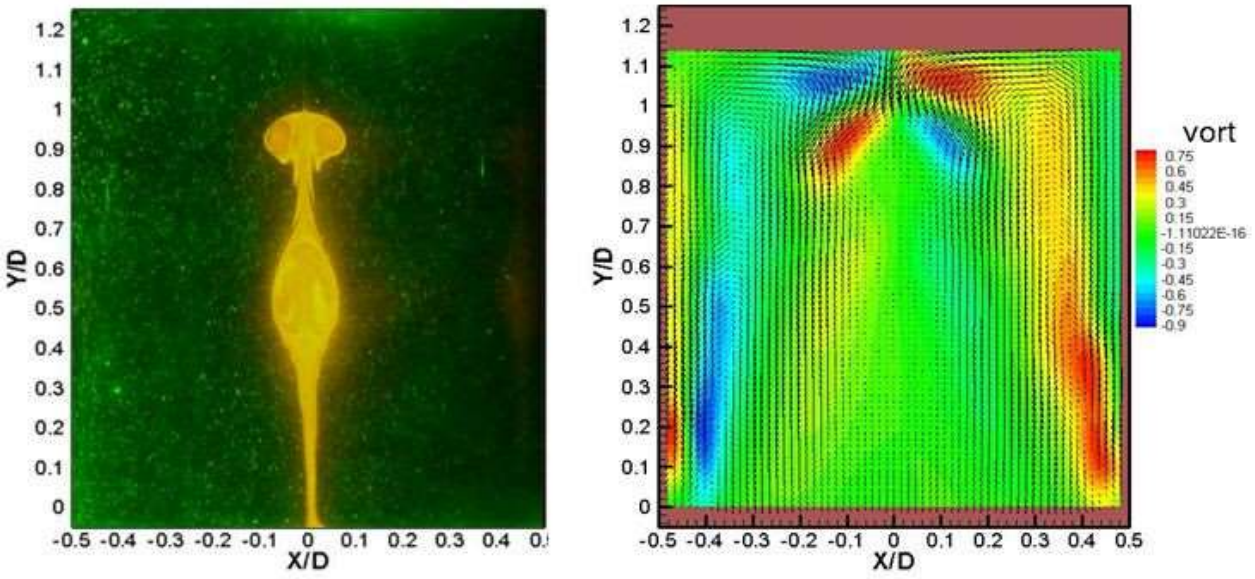

Figure 6: (a) Dye flow visualization (b) Vorticity contours along with velocity vector of global flow at *Re* = 2359 for *AR* = 2.5

Blue color in all figures denotes the clockwise rotation whereas red color denotes counter clockwise rotation. At this rotational Re, upstream and downstream *VB* bubbles appear at a distance of 0.8D (115 *mm*) and 0.4D (60 *mm*) respectively from the bottom disk (figure 6(b)). Upstream and downstream *VB* bubbles are 0.3D (28 *mm*) and 0.1D (14 *mm*) in size respectively (figure 6). Upstream *VB* bubble has two counter rotating re- circulation zones which are 0.15D (21 *mm*) in size. Downstream *VB* bubble is more stretched in axial direction not in radial direction and this bubble also has one pair of oscillating vortices. Two stagnation points are located at distance of D (140 *mm*) and 0.6D (84 *mm*) from the bottom disk as shown in figure 6 (b). As the rotation rate is increased the size of *VB* bubble increases, downstream stagnation point moves towards the upstream stagnation point and upstream *VB* bubble moves towards the non-rotating disk.

For *AR* = 3.5, PIV results in the form of vorticity, axial and radial velocity contours for rotational *Re* = 2798 are shown in figure 7. Vorticity contours shown in figure 7 (b) denote that the size of upstream *VB* is smaller than the size of downstream *VB*. At this rotational *Re*, upstream and downstream *VB* bubbles appear at a distance of 1.2D (168 *mm*) and 0.3D (42 *mm*) respectively from the bottom disk (figure 4.10 (b) and (d)). Upstream and downstream *VB* bubbles are 0.1D (14 *mm*) and 0.2D (28 *mm*) in size respectively (figure 7 (d)). Upstream *VB* bubble has two counter rotating recirculation zones which are 0.05D (7 *mm*) in size. There are two downstream *VB* bubbles which are more stretched in the axial direction. Two stagnation points are located at distance of 1.4D (195 *mm*) and 0.9D (130 *mm*) from the bottom disk as shown in figure 4.10 (c). As the rotation rate is increased size of *VB* bubble increases, downstream stagnation point moves towards the upstream stagnation point and upstream *VB* bubble moves towards the non-rotating disk. At this high *AR* flow becomes unsteady with the increment in rotation rate.

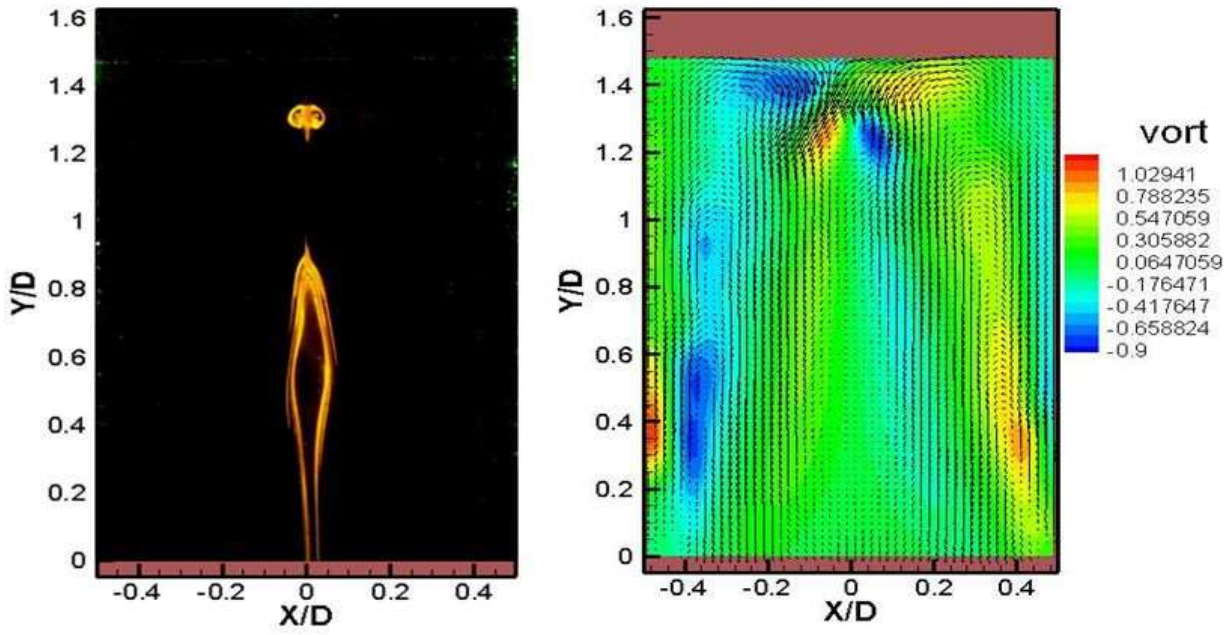

Figure 7: (a) Dye flow visualization (b) Vorticity contours along with velocity vector of global flow at *Re* = 2798 for *AR* = 3.

4 Conclusion

The results presented here characterize the different flow behavior in the central part of the closed cylindrical flow with rotating bottom disk in the range of $AR \leq 3.50$ and $Re \leq 3500$. For $AR < 1.95$ only single vortex breakdown is observed, Two breakdowns occurred for the range $1.95 < AR < 3.25$ and three breakdown occurred in succession in the neighborhood of $AR = 3.4$ over a limited range of conditions. For a particular value of aspect ratio breakdowns are only observed between certain values of Reynolds number. Detailed analysis of PIV data and control of vortex breakdown is currently under progress.

Acknowledgements

We are thankful to all the supporting staff & students of low speed aerodynamics lab, Department of Aerospace Engineering-IIT Kanpur, TSI Instruments-Bangalore; for their continuing help and support in conducting the experiments.

References

Brøns Morten, et al. (2007) The influence of imperfections on the flow structure of steady vortex breakdown bubbles. *Journal of Fluid Mechanics* 578: 453-466.

Escudier MP (1984) Observations of the flow produced in a cylindrical container by a rotating end wall. *Experiments in fluids* 2.4: 189-196.

Mullin T, Kobine JJ,Tavener SJ, and Kliffe CA (2000) On the creation of stagnation points near a straight and sloped walls. *Physics of Fluids* 12: 425-432

Husain Hyder S, Vladimir Shtern, and Fazle Hussain (2003) Control of vortex breakdown by addition of near-axis swirl. *Physics of Fluids* 15.2: 271-279.

Leibovich Sidney (1978) The structure of vortex breakdown. *Annual review of fluid mechanics* 10.1: 221-246.

Spohn AM, Mory, Hopfinger EJ (1993) Observations of vortex breakdown in an open cylindrical container with a rotating bottom. *Experiments in Fluids* 14.1: 70-77.

Vogel Horst Udo (1968) Experimentelle Ergebnisse über die laminare Strömung in einem zylindrischen Gehäuse mit darin rotierender Scheibe. *Dissertation Göttingen, Univ.,* MPIStrömungsforschung,